Construction and Building Materials 25 (2011) 1772–1788

Contents lists available at ScienceDirect

Construction and Building Materials

journal homepage: www.elsevier.com/locate/conbuildmat

In-plane retrofitting of masonry panels with fibre reinforced composite materials

Bibiana Luccioni [a,*], Viviana C. Rougier [b]

[a] Structures Institute, National University of Tucumán, CONICET, Av. Roca 1800, 4000 S.M. de Tucumán, Argentina
[b] National Technological University, Reg. Fac. C. del Uruguay, GMN, Ing. Pereira 676, Concepción del Uruguay, Argentina

ARTICLE INFO

Article history:
Received 2 February 2010
Received in revised form 1 October 2010
Accepted 13 November 2010
Available online 18 December 2010

Keywords:
Masonry
Fibre reinforced polymers
Composites
Retrofitting
Repair

ABSTRACT

Research activities carried out during the past years concerning the use of fibre reinforced polymers (FRP) as external reinforcement of masonry walls have shown that this system considerably improves structural stability and ductility with minimum increase in the load transmitted to foundations. However, different aspects of this retrofitting system should still be analyzed.

The mechanical behaviour under in-plane compression and diagonal compression of clay masonry panels reinforced or repaired with carbon fibre reinforced polymer laminates is experimentally assessed in this paper. The results show that if correct retrofitting schemes are chosen, reinforcement and repairing with fibre reinforced polymers improves masonry behaviour, increasing ductility and, in some cases, ultimate strength and even stiffness. In this way, brittle behaviour and sudden failure of unreinforced masonry can be avoided.

© 2010 Elsevier Ltd. All rights reserved.

1. Introduction

Several reinforcing and retrofitting methods for masonry walls have been studied in recent years. Among them, the construction of additional reinforced concrete frame elements contributing to reduce the loads on the walls or surface treatments that involve reinforcement bars and the addition of a concrete cover are commonly used. These retrofitting techniques often add a significant mass to the structure, consume time, have high construction costs and are not reliable in many cases [1]. Studies performed after the Northridge Earthquake (1994) showed that 450 buildings reinforced before the earthquake failed after it [2].

Consequently, the study of new materials and techniques for the efficient retrofitting of damaged masonry structures is extremely necessary. Recent advances in the polymeric fibre reinforced composite materials (FRP) field have lead to the development of new materials for the retrofitting of masonry structures in areas where conventional materials have failed [1]. Research activities developed by different authors to investigate the in-plane and out-of-plane behaviour of masonry panels made of clay bricks [2–25] or concrete blocks [26–30] and strengthened with composites have shown that polymer reinforced composites give a light and efficient alternative to traditional materials and improve the behaviour of masonry elements under monotonic, seismic and explosive loads. From the structural point of view, dynamic properties of the structure are not altered since the added mass and stiffness are negligible. This fact is of fundamental importance for the reinforcement of structures that could be subjected to moderate or severe earthquakes, since any increase of mass or stiffness leads to an increase of seismic forces.

Although the efficiency of retrofitting techniques using fibre reinforced composite materials has been experimentally proved, a better description of the mechanical behaviour of reinforced masonry under different load conditions should be obtained in order to improve intervention techniques. There are many recent experimental and numerical research works related to the retrofitting of masonry walls with different types of FRP [23]. In fact, in the last decades, some analytical methods [30–32] have been proposed and numerical tools based on non-linear models implemented in finite elements codes are currently the most common advanced strategies to simulate the structural behaviour of masonry structures [13,14,24,33–36].

In spite of this effort, it is still difficult to obtain reinforcing and/or retrofitting effective criteria that cover strength, stiffness, ductility, durability and bond criteria from available theories and design methods usually used in engineering practice.

An experimental study of the mechanical behaviour of clay brick masonry elements under in-plane increasing loads is presented in this paper. The study is mainly oriented to the identification of the elementary mechanisms involved in the response of masonry elements retrofitted with carbon fibre reinforced polymers (CFRP). Masonry specimens are reinforced or repaired with CFRP. The paper is complemented with the results of numerical simulation that contributes to the analysis of retrofitting bond length effect. The results presented in the paper could help in the understanding of the overall mechanisms introduced by the reinforcement.

* Corresponding author.
E-mail address: bluccioni@herrera.unt.edu.ar.edu.ar (B. Luccioni).
URL: http://www.herrera.unt.edu.ar/iest (B. Luccioni).

0950-0618/$ - see front matter © 2010 Elsevier Ltd. All rights reserved.
doi:10.1016/j.conbuildmat.2010.11.088

2. Brief literature review of in-plane behaviour of reinforced masonry

2.1. Behaviour of reinforced masonry under compression

Some authors have studied the behaviour of reinforced masonry under normal and parallel to bed joint compression. The more significant results obtained for hollow concrete block masonry [29], and clay brick masonry [16] are presented in this section.

2.1.1. Hollow concrete masonry walls

According to a recent research by El-Dakhakhni et al. [29] on small masonry specimens made with hollow concrete blocks subjected to uniaxial compression normal and parallel to the bed joint, the reinforcement with FRP not only increases the strength but also increases the ductility preventing out of plane brittle failure and keeping the wall integrity even after significant structural damage.

2.1.2. Clay masonry walls

Prakash and Alagusundaramoorthy [16] studied the effectiveness of glass fibre reinforced polymers (GFRP) retrofitting on the behaviour of masonry *wallettes* subjected to compression normal and parallel to bed joint. GFRP retrofitting increased the strength and stiffness of *wallettes* but the average ultimate strain was significantly reduced.

2.2. Behaviour of reinforced masonry under shear

Shear reinforcement of masonry walls with FRP has also been studied on concrete block masonry and on clay brick masonry.

2.2.1. Hollow concrete masonry walls

El-Dakhakhni et al. [29] investigated the effects of FRP laminates on altering the failure mode and strength and deformation characteristics of small specimens subjected to diagonal tension and joint shear. From the experimental program, the authors concluded that laminates significantly increased the load-carrying capacity of the masonry assemblages exhibiting shear failures along the mortar joints. The average joint shear strength of the retrofitted specimens was equal to eight times that of their unretrofitted counterparts. The values of the coefficients of variation for the retrofitted assemblages were generally lower than those of the unretrofitted specimens. This result demonstrates the laminate's role in reducing strength anisotropy and variability of unreinforced masonry.

2.2.2. Clay masonry walls

Shear behaviour of retrofitted clay masonry has been studied at different scales.

Experimental and numerical modelling at the elementary level has been receiving increasing interest [23]. Eshani and Saadatmanesh [3], Roca and Araiza [23] and Luccioni and Rougier [24], among others, investigated the efficiency of external shear reinforcement of small specimens made by three solid bricks and two joints. The retrofitting with unidirectional CFRP bands oriented orthogonal to the joints increases the shear strength. The anchorage length of the CFRP band is a very important variable in the design of the shear reinforcement. Strength increases with the length of the bands. In general, the failure is produced by the failure of the bricks surface producing the debonding of the CFRP laminas. The bond behaviour of FRP reinforcement on clay bricks has been investigated in many papers and numerical approaches to model the masonry-FRP interface behaviour have been recently proposed [19,21,35,36].

Valluzzi et al. [9] and Gabor et al. [14] performed the diagonal compressive test to investigate the in-plane shear response of small brick masonry panels strengthened with FRP laminates. From the results obtained by Valluzzi et al. [9] and Gabor et al. [14] on panels made of solid and hollow clay bricks, respectively, it can be concluded that fibre reinforced polymer reinforcement increases shear strength and ductility depending on the reinforcement scheme, it increases the stiffness, especially in solid brick masonry, and prevents brittle failure only for specimens with the reinforcement covering all their surfaces.

ElGawady et al. [2,18] studied the response of half scale masonry panels strengthened with FRP laminates applied diagonally to the joints subjected to both static and cyclic loading. The increase in the lateral strength was proportional to the amount of FRP axial rigidity. However, using high amount of FRP, axial rigidity led to very brittle failure. Similar tests were reported by Santa María et al. [15].

Many researchers have also studied the seismic reinforcement with fibre reinforced polymers of half [2] and full-scale [11,15,37,38] masonry walls made of hollow clay bricks. It was observed that the reinforcement improves lateral stability of the walls [2], increases the shear strength of the walls, the maximum displacement before failure and the displacement and load of first major crack [15]. Seismic retrofitting of unreinforced masonry walls with FRP proved to be an effective and reliable strengthening alternative [11].

3. Tests description

3.1. Introduction

Two groups of similar panels were constructed and tested according INPRES-CIRSOC 103 specifications [25]: Group I ($580 \times 610 \times 130$ mm panels) and Group II ($560 \times 550 \times 125$ mm panels). The dimensions of the specimens differ due to the different dimensions of the solid clay bricks used. All panels had a 15 mm thick mortar joint.

Panels were constructed following INPRES-CIRSOC 103 [25] recommendations and trying to reflect material and workmanship qualities similar to those used in actual masonry construction in Argentina.

The specimens were tested under uniaxial compression normal and parallel to the bed joints and diagonal compression. For comparison, some of the specimens were tested up to failure without reinforcement, others were reinforced with CFRP and tested up to failure and others were tested until a predefined degree of damage (specified latter for each kind of test), then they were unloaded and repaired with woven carbon fabric, laminated and bonded on site and, finally, they were tested again up to failure. For the design of the FRP strengthening of the panels no guideline was available when tests were conducted. Because of that, a finite element analysis with different retrofitting configurations was carried out [42]. The objective of that numerical analysis was both assessing the influence of the different reinforcement schemes on masonry and obtaining the best arrangement.

All the tests were performed under increasing load with displacement control. The loading rate was chosen according to the different types of tests. For compression normal to the bed joints it was not expected to have a sudden failure so a 0.01 mm/s loading rate was chosen in order to have a quasistatic test with a total duration of 15 min. This loading rate had been proved to be adequate for the bricks previously tested under uniaxial compression. The loading rate was decreased to 0.008 mm/s for compression parallel to bed joint and diagonal compression tests because a sudden failure was expected to occur.

Table 1
Mortar and bricks mechanical properties obtained from tests.

Properties	Mortar			Bricks	
	Group I		Group II	Group I	Group II
	(a)	(b)			
Elasticity modulus E (MPa)	3380	4312	1528	1662	1400
Comp. ult. strength, σ_{uc} (MPa)	6.73	7.72	4.00	11.82	8.28
Charac. Flex. Rup.Modulus (MPa)	2.83	2.83	2.65	–	–
Poisson ratio, ν	0.21	0.21	0.21	0.16	0.15
Dimensions (mm):					
Length	–	–	–	280	260
Width	–	–	–	130	125
Height	15	15	15	50	55

Table 2
Mechanical properties of carbon fibre reinforced epoxy lamina (SIKA).

Elasticity modulus, E (MPa)	72,500
Tension strength, σ_t (MPa)	960.0
Poisson ratio, ν	0.2
Ultimate tension strain (%)	1.33
Thickness (mm)	1.0
Weight (g/m^2)	183.0

3.2. Materials

3.2.1. Mortar

Mortar used in panels construction was designed according to INPRES-CIRSOC 103 [39] prescriptions, in order to obtain a characteristic compressive strength of 5 MPa at an age of 28 days, which corresponds to a Type N mortar (mix design of 1:1:5 ratio, cement: lime: sand, by volume). The water quantity added to the dry mixture was determined to ensure a good workability of the fresh mortar.

Following IRAM standards [40] flexure and compression tests were performed to obtain the mechanical properties of mortar presented in Table 1. Among the specimens of Group I, two similar mortars can be distinguished: (a) and (b). Mortar (a) was used for specimens of Group I tested under compression normal and parallel to bed joints, while mortar (b) was used for specimens of Group I subjected to diagonal compression. The ultimate strength values correspond to the mean of 20 half test specimen of $40 \times 40 \times 160$ mm for each type of mortar.

3.2.2. Bricks

Slightly different types of clay bricks were used for Groups I and II. The dimensions of the bricks for Groups I and II are included in Table 1.

Mechanical properties of the bricks were obtained from tests following IRAM standards [41]. The strength, elasticity modulus and Poisson ratio mean values of the two types of bricks used in the tests are also presented in Table 1. They are the mean of 20 tests in each case.

3.2.3. Carbon fibre fabric

Unidirectional carbon fibre fabric with high content of carbon and high modulus and strength, saturated in situ with an epoxy system was used for the reinforcement and retrofitting. The properties of the lamina were obtained from the manufacturer (SIKA) specifications and were numerically validated [42] using a constitutive model for unidirectional fibre reinforced lamina. They are presented in Table 2.

In order to remove mortar remains, the surfaces of the panel were carefully polished with a steel brush and high-pressure air. The carbon fibre fabric soaked up with the epoxy resin was applied to both panel surfaces previously impregnated with the same resin. In all cases, one CFRP lamina of 1 mm final thickness was applied to each surface of the panel.

3.3. Uniaxial compression tests

The specimens tested are described in Table 3. Specimens MN1–MN11 were tested under compression normal to the bed joint while specimens MP1, MP2 and MP3 were subjected to compression

Table 3
Panels tested under uniaxial compression.

Specimen	Group	Retrofitting/repairing scheme	Failure mode
MN1	Ia	–	Vertical cracks on front and back sides
MN2	Ia	–	Vertical cracks on front and back sides
MN3	Ia	–	Vertical cracks on front and back sides
MN6	II	–	Vertical cracks on front and back sides and crushing near supports
MN7	II	–	Vertical cracks on front and back sides and crushing near supports
MN8	II	–	[a]
MN11	II	–	[a]
MN4Ret	Ia	Totally retrofitted	Vertical cracks all along the lateral vertical sides
MN5Ret	Ia	Ret 75 mm × 580 mm strips	Small vertical cracks in front, back and vertical sides
MN8Rep	II	Rep 75 mm × 560 mm strips	Failure of bricks with pull out of the composite lamina
MN9Ret	II	Ret 75 mm × 560 mm strips	Small vertical cracks in front, back and vertical sides
MN11Rep	II	Rep 75 mm × 560 mm strips	Failure of bricks with pull out of the composite lamina
Compression parallel to the bed joints			
MP1	Ia	–	Sudden with brick rows debonding
MP2	Ia	–	Sudden with brick rows debonding
MP3	Ia	–	Sudden with brick rows debonding

Ret: retrofitted; Rep: repaired; N: compression normal to bed joint; P: compression parallel to bed joint.
[a] No failure mode because they were unloaded before failure and repaired.

Fig. 1. Compression test setup. (a) Normal to the bed joint (MN1, MN2, MN3, MN6, MN7). (b) Parallel to the bed joint (MP1, MP2, MP3).

parallel to the bed joint. The test setups for compression normal to the bed joint and parallel to the bed joint are shown in Fig. 1. A rubber layer of approximately 8 mm thickness was inserted between the supports and the upper and lower faces of the specimen in order to reduce the lateral restraint. Vertical and horizontal relative displacement between two fixed points were measured on both sides of the panels and then extrapolated to the total width and height of the panel. Stress–strain curves were derived from load–displacements measurements. In most cases, the measurement equipment had to be removed before failure for safety reasons.

3.3.1. Retrofitted specimens

In order to assess the effectiveness of CFRP retrofitting technique, three reinforced masonry panels were tested under compression normal to the bed joints. The two types of retrofitting schemes shown in Fig. 2 and described in Table 3 were used: total reinforcement and reinforcement with 75 mm width strips. The strip width was chosen based on numerical results [42]. In all cases, both the front and back sides of the panels were reinforced with one CFRP layer and fibres were laid out horizontally, that is, parallel to the bed joints and normal to the load direction.

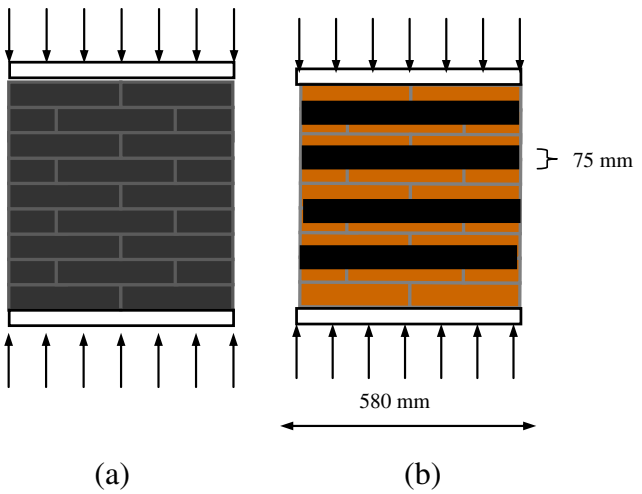

Fig. 2. CFRP retrofitted and repaired specimens tested under compression. CFRP layout. (a) Completely reinforced (MN4Ret). (b) Band reinforced (MN5Ret).

3.3.2. Repaired specimens

In order to assess the efficiency of the repairing with CFRP, two specimens (see Table 3) were tested under uniaxial compression up to approximately 70% of the failure load, when the first cracks could be observed and then unloaded. The panels were repaired with 75 mm width CFRP bands and they were tested again up to failure (MN8Rep and MN11Rep). In all cases, both front and back faces of the panels were repaired with one layer of CFRP bands and fibres were laid out horizontally, that is, parallel to bed joints and normal to load direction. The layout of the CFRP strips and the number of layers is the same than that used for the retrofitting scheme, see Fig. 2b.

3.4. Diagonal compression tests

The set of unreinforced, retrofitted and repaired masonry panels briefly described in Table 4 was tested under diagonal compression. The test specimens were built following the specifications in INPRES-CIRSOC 103 [39] for the evaluation of masonry shear strength. According to these prescriptions [39], test panels should be square and with l greater than 550 mm. In order to apply the compression loading, the corners of the panels should be embedded in two metallic supports with embedding length r greater or equal to 200 mm. The test setup and measurement devices arrangement used for diagonal compression tests are shown in Fig. 3. A rubber layer was also inserted between the specimens and the metallic supports to reduce friction between them and the specimens. Nevertheless, in some cases it has been observed that this type of support has an undesirable effect because it can cause a localized failure in coincidence with one of its ends, which spreads, producing an anticipated collapse. Gabor et al. [13] analyzed the influence of two boundary conditions, $r = l/10$ and $r = l/6$ on the behaviour of the masonry panel. For the former they obtained a localized failure at one of the bearing zones, while for the latter a generalized failure was obtained.

Table 4
Panels tested under diagonal compression.

Specimen	Group	Retrofitting/repairing scheme	Failure mode
MD1	Ib	–	Joint sliding
MD2	Ib	–	Mixed: Bricks failure with joint sliding
MD3	Ib	–	Mixed: Bricks failure with joint sliding
MD7	II	–	Failure due to diagonal tensions and sliding
MD8	II	–	[a]
MD12	II	–	[a]
MD3Rep	Ib	Rep 70 mm strips orthogonal to load. Central band length: 640 mm	Brick failure near supports and pull out of CFRP band
MD4Ret	Ib	Completely retrofitted	Crushing in support zone
MD5Ret	Ib	Ret 50 mm strips orthogonal to load. Central band length: 640 mm	Bricks failure near supports
MD6 Ret	Ib	Ret 50–60 mm strips/bed joints. Central band length: 640 mm	Bricks failure near supports with sliding of central mortar joint
MD7Rep	II	Rep 70 mm strips orthogonal to load. Central band length: 640 mm	Brick failure near supports and pull out of CFRP band
MD8Rep	II	Rep 70 mm strips orthogonal to load. Central band length: 640 mm	Brick failure near supports and pull out of CFRP band
MD9Ret	II	Ret 70 mm strips orthogonal to load. Central band length: 640 mm	Central band pull out and sliding of mortar joints
MD10Ret	II	Ret 70 mm strips orthogonal to load. Central band length: 640 mm	
MD11Ret	II	Ret 70 mm strips orthogonal to load. Central band length: 320 mm	Bricks and mortar failure localized near supports. Central band pull out
MD12Rep	II	Rep 70 mm strips orthogonal to load. Central band length: 640 mm	Brick failure near supports and pull out of CFRP band
MD13Ret	II	Ret 70 mm strips orthogonal to load dir. Central band length: 400 mm	Bricks and mortar failure localized near supports. Central band pull out

Ret: retrofitted; Rep: repaired; D: diagonal compression.
[a] No failure load because they were unloaded before failure and repaired.

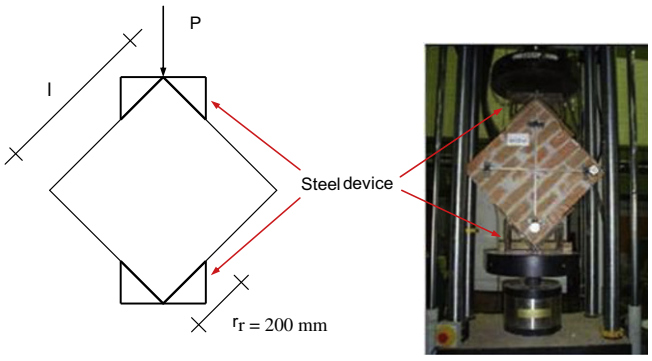

Fig. 3. Diagonal compression test setup and measurement devices arrangement.

Relative displacements along the compressed diagonal and tensioned diagonal were recorded between two fixed points located along the diagonal and were later extrapolated to the total length of the diagonals to obtain the total diagonal displacements.

3.4.1. Panels retrofitted with CFRP laminas

Three different possible retrofitting layouts presented in Fig. 4 were studied: total reinforcement with fibres laid out normal to load direction, diagonal strips bonded orthogonally to the compressive diagonal and strips parallel to the bed joint. One layer of CFRP was used in each face of the specimens in all cases. The different specimens tested are specified in Table 4.

In order to study the effect of bond length on the retrofitting effectiveness, four additional specimens of Group II, retrofitted with CFRP diagonal strips of variable length, were tested under diagonal compression. Only the length of the central band was varied (640 mm, 400 mm, 320 mm). The description of the specimens is presented in Table 4.

3.4.2. Panels repaired with CFRP laminas

In order to assess the efficiency of CFRP laminas as a repairing material, four damaged panels (MD3, MD7, MD8 and MD9) were repaired and then tested again. To produce previous damage specimens MD3 and MD7 were loaded under diagonal compression up to failure while specimens MD8 and MD12 were loaded up to 50% of the expected failure load and no damage could be visually observed in this case.

The cracks were first filled in with cement paste and then the CFRP laminas were adhered to the panels. All the specimens were repaired with diagonal CFRP strips of 70 mm width on the front and back faces of the panels with a layout similar to that presented in Fig. 4b.

The repaired specimens were reloaded up to failure under diagonal compression.

4. Discussion of test results

4.1. Uniaxial compression tests

4.1.1. Unreinforced specimens

Fig. 5 shows the experimental relationships between the compressive strength σ_c, and both transverse ε_t and axial ε_l strains of some of unreinforced panels tested under compression normal and parallel to bed joints. Ultimate load values were also included in Fig. 5.

For compression normal to bed joints a relatively linear relationship between compressive stress and axial strain, with low values of the lateral strain is observed up to about 50% of the peak strength. Then, a sudden increase in lateral strain and stiffness degradation due to vertical cracks is observed. The integrity of the panels is preserved during the softening part of the stress–strain curve up to the complete failure. Failure is not sudden but ductile even though crushing of the bricks near the loading plates is observed in some cases. Failure pattern is presented in Fig. 6. Vertical cracks all along both sides of the panels are evident.

The influence of mortar properties in the specimen's response to compression normal to bed joints is also clear in Fig. 5. The curve corresponding to MN3 shows greater stiffness and strength and this difference is mainly due to the greater stiffness and strength of the mortar (see Table 1). As a counterpart, it may be observed that increasing mortar strength leads to a more brittle behaviour. For specimens MN1 and MN2 only the ultimate load was recorded. The values obtained were 192 kN and 262 kN, respectively.

For compression parallel to bed joints, three panels were tested but displacement measurements could be recorded only for one of them due to the sudden and brittle failure obtained in this type of test. However, ultimate load was recorded for all specimens with a mean value of 264 kN. Experimental stress–strain curve is plotted up to 80% of the ultimate strength

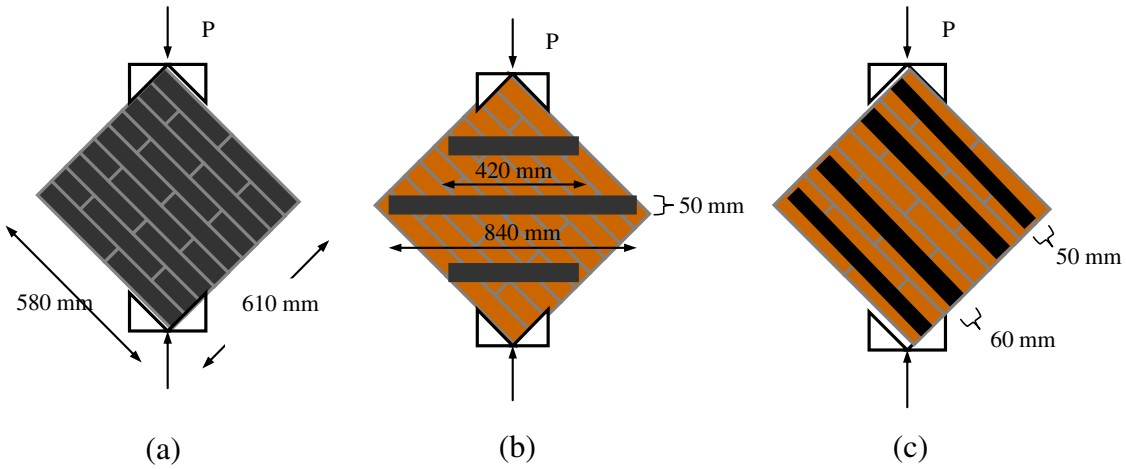

Fig. 4. CFRP layout and failure patterns of retrofitted panels under diagonal compression. (a) Completely retrofitted. (b) Retrofitted with diagonal bands. (c) Retrofitted with bands parallel to mortar joints.

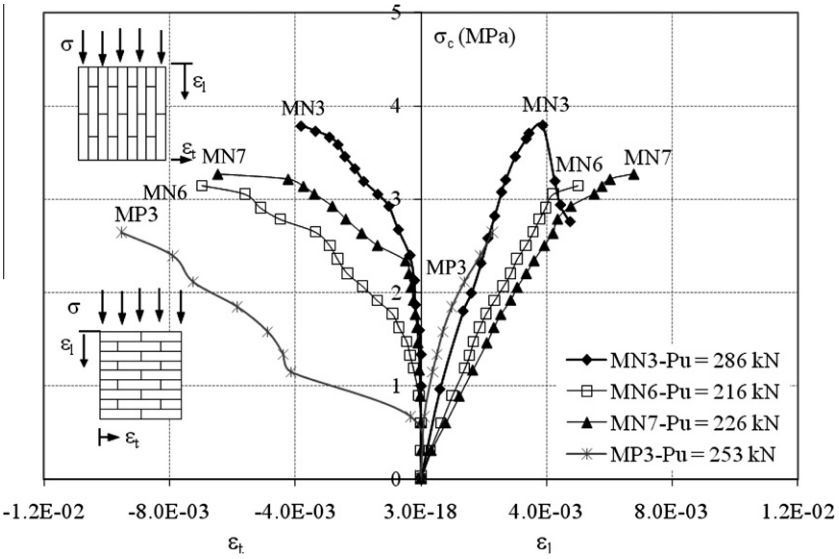

Fig. 5. Stress–strain curves for unreinforced specimens under compression.

Fig. 6. Compression test failure pattern. (a) Normal to the bed joint (MN1, MN2, MN3, MN6, MN7). (b) Parallel to the bed joint (MP1, MP2, MP3).

(Fig. 5). Failure initiates for nearly 20% of the ultimate strength, due to the positive deformation of the mortar joints orthogonally to the applied load. The sudden increase in transverse strains in Fig. 5 corresponds to the opening of the mortar joints and the later separation of a complete row of bricks. Then, the resulting brick columns continue supporting load. A sudden failure with bricks and mortar spoliation, as shown in Fig. 6b, is obtained. Debonding of brick from the mortar is evident in Fig. 6b.

4.1.2. Retrofitted specimens

Stress-axial and transverse strain ($\sigma - \varepsilon_l$ and ε_t) curves under compression normal to the bed joint for retrofitted specimens are presented in Fig. 7. The curves for specimens of the same groups but without reinforcement are also included in Fig. 7 for comparison. Additionally the ultimate load values are shown in Fig. 7. In the case of the completely reinforced panel, only the axial displacements were recorded. Although none of the retrofitted specimens tested show a considerable increase in strength under compression normal to the bed joints, a more ductile behaviour is obtained for retrofitted panels when compared to unreinforced panels.

The improvement in compression strength of retrofitted specimens in comparison with reference specimens is presented in Fig. 8. The reinforcement ratio ρ in one direction is defined as a percentage of the total cross sectional area of FRP in that direction over the corresponding gross sectional area of the panel [9]. The strength increase is about 22% for the full retrofitted specimen, 12% for specimen MN5Ret and 5% for panel MN9Ret, both retrofitted with CFRP strips.

An increase in axial deformation capability of about 240% is obtained for the totally reinforced panel while this increase decays to 12% and 22% for the specimens reinforced with strips, MN5Ret and MN9Ret respectively (see Fig. 7). A slight increase in stiffness can also be perceived for the completely reinforced specimen, MN4Ret, and MN9Ret, retrofitted with strips. Sudden increase in transverse strains, corresponding to the opening of the mortar joints, is prevented with CFRP strips retrofitting.

The failure patterns obtained for the different specimens tested are shown in Fig. 9 and they are described in Table 3. For total reinforcement, no crack can be observed in front and back sides, while vertical cracks appear in lateral sides. The failure is more ductile than for unreinforced specimens and the integrity of the panel is preserved even after it is removed from the test machine. The panels that were reinforced with strips show small vertical cracks in the front, back and lateral sides. The failure of the superficial layers of the bricks produc the pulling out of the CFRP lamina, as it can be observed in Fig. 9. The failure is less ductile than for the case of total reinforcement and similar to that of unreinforced panels. In no case, failure of the CFRP laminate was observed.

4.1.3. Repaired specimens

The stress-axial and transverse strain ($\sigma - \varepsilon_l$ and ε_t) curves for repaired specimens are presented in Fig. 10.

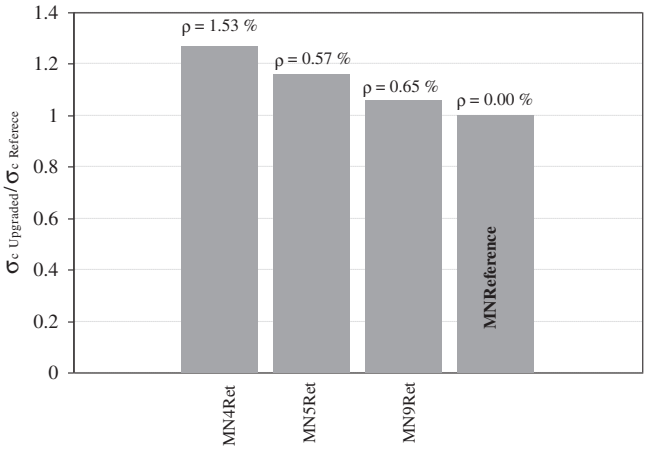

Fig. 8. Improvements in compression strength of retrofitting specimens.

An increase in vertical stiffness due to the repairing can be observed. In the case of MN8Rep the increase in stiffness is almost negligible in comparison with MN11Rep. These results could be attributed to the variability of properties in masonry itself. More tests should be conducted in order to explain the differences observed.

The initial strength is just recovered. Only a small strength increase (10%) was achieved for the specimen MN11. Unlike initially reinforced specimens, in this case, no increase in the deformation capacity is observed.

The failure pattern obtained is shown in Fig. 11. The failure of the repaired specimens is due to the crushing in the upper support zone that produced the pulling out of the composite lamina including the surface layers of the bricks. No cracks in the front and back sides of the panels can be observed.

4.2. Diagonal compression tests

4.2.1. Unreinforced masonry panels

The load–displacement ($P - \delta_l$ and δ_t) curves for the unreinforced specimens MD3 and MD7 are presented in Fig. 12. Specimen MD7 shows greater deformation capacity mainly due to the differences in mortar properties (see Table 1). The global behaviour

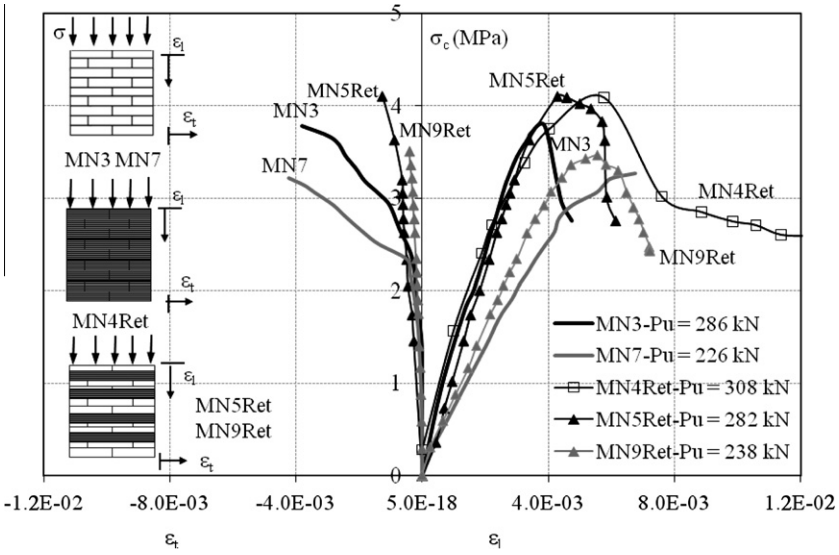

Fig. 7. Stress–strain curves for CFRP retrofitted specimens under compression.

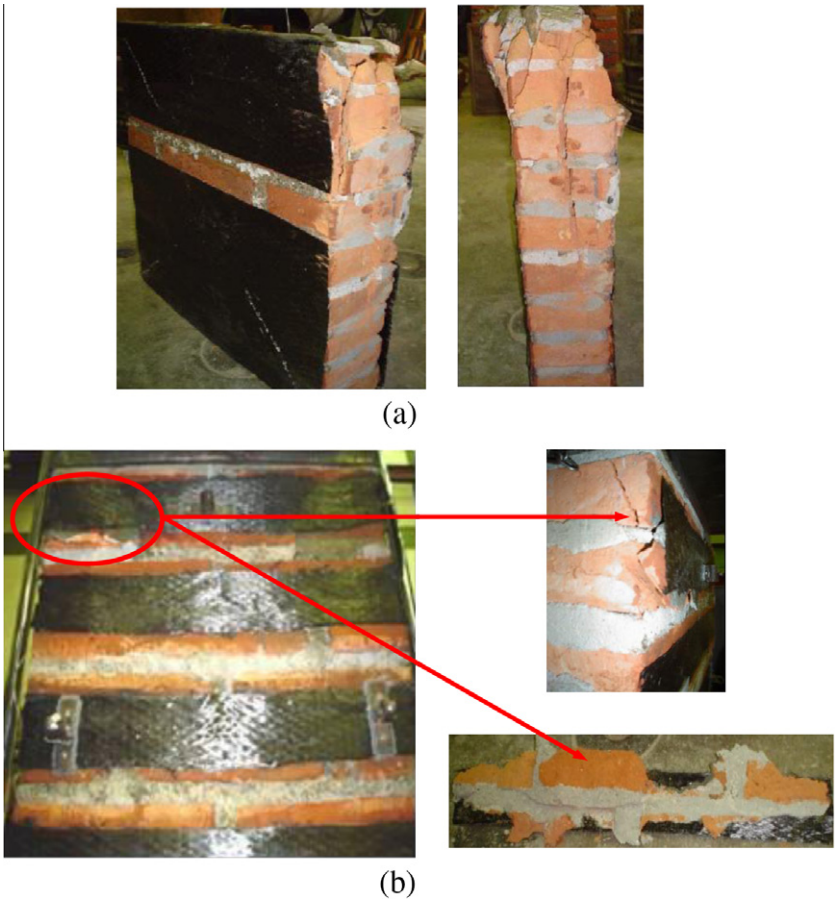

Fig. 9. CFRP retrofitted and repaired specimens tested under compression. Failure mode. (a) Completely reinforced (MN4Ret). (b) Band reinforced (MN5Ret).

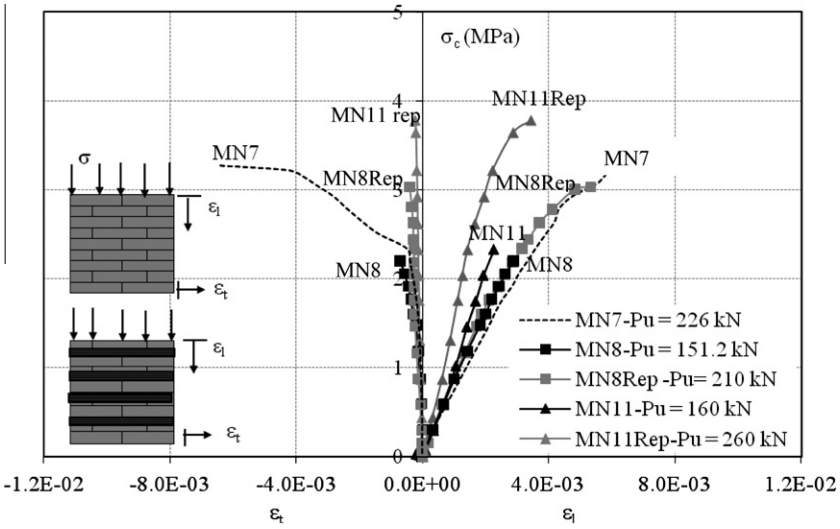

Fig. 10. Stress–strain curves for CFRP repaired specimens under compression.

described by curve representing the applied load as a function of the displacement along the compressed diagonal, is quasi- elastic up to failure load. Ultimate load values are also included in Fig. 12.

The failure patterns of specimens MD1, MD3 and MD7 are presented in Fig. 13. In all cases, a brittle failure with bricks breakage and sliding of mortar joints is achieved. Panel MD1 fails due to the sliding of mortar joint at a load of 50.50 kN. In the case of panel MD3, it is clear that failure is initiated in the upper support at a load of 82.90 kN. In the case of MD7 failure is produced by the formation of a crack along the compressed diagonal and it is less brittle than for the other cases. The ultimate load attained is 85.20 kN. In general, the type of failure is strongly dependent on the bond strength between mortar and bricks.

Fig. 11. Compression normal to the bed joint of CFRP repaired specimens. Failure mode.

4.2.2. Panels retrofitted with CFRP laminas

The load–displacement ($\widetilde{P} - \delta_l$ and δ_t) curves for retrofitted panels under diagonal compression are included in Fig. 12 for comparison with those for unreinforced specimens are also included in Fig. 12 for comparison. In all cases, the measurement equipment was removed before ultimate load was attained to preserve it from breakage due to sudden failure.

Fig. 12 shows that the total reinforcement significantly increases the stiffness and the strength of the panel. This effect should be considered or modelled when assessing, for example, seismic behaviour of the retrofitted structure.

No appreciable increase in stiffness is obtained with diagonal strips but, as it can be observed in Fig. 12, the ultimate load is practically duplicated with a significant saving of CFRP material. Thus the increase of strength is quite remarkable while stiffness is kept practically unmodified. No improvement is achieved with CFRP strips parallel to mortar joints.

Different failure modes shown in Fig. 14 are obtained for the different retrofitting schemes. In the case of total reinforcement, the integrity of the specimen is preserved without evidence of cracks near to failure load. Failure is produced by the brick crushing near the upper support. Specimen retrofitted with diagonal strips fails due to detachment of the superficial layers of the bricks. This failure is initiated near the upper support and propagates to the lower support. The behaviour is less brittle than for unreinforced specimens and the predicted increase in ultimate strength is obtained. A brittle failure initiated in the support and followed by the sliding of central mortar joint is observed in the case of the specimen MD6Ret retrofitted with strips parallel to the bed joints. The stress concentration in the support produces the separation of the superficial layers of the bricks with consequent pull out of the composite lamina. Consequently, the specimen presents an abrupt failure and the expected strength increase is not attained.

The load–displacement curves for the specimens retrofitted with different CFRP strip lengths and the comparison with the unreinforced panel are presented in Fig. 15. In general, strength increases with the increase in the central band length but the

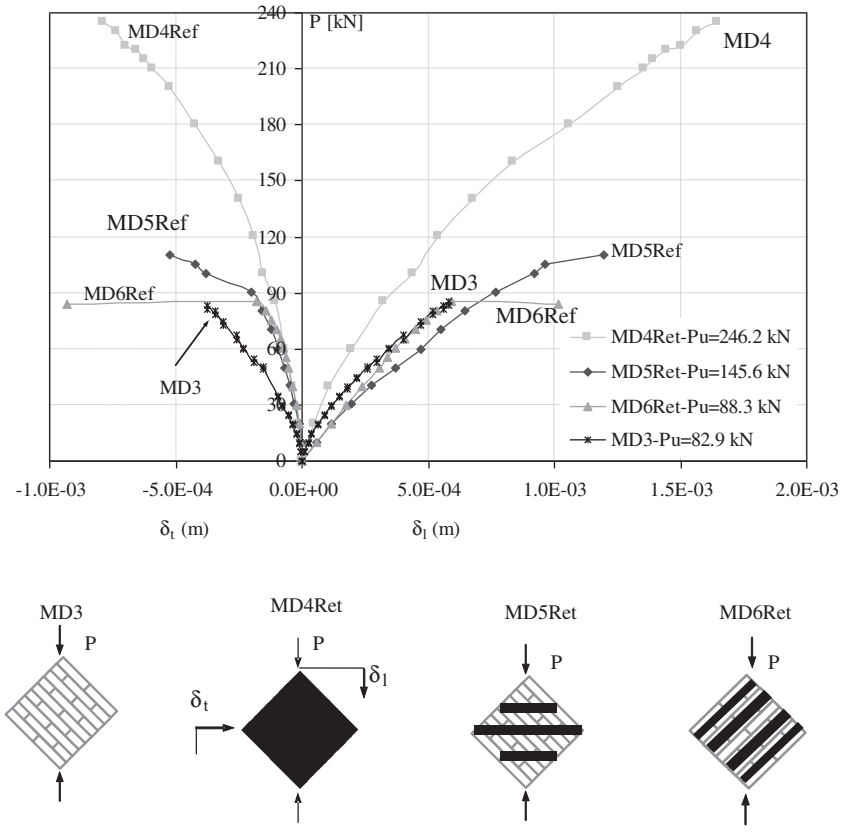

Fig. 12. Load–displacement curves under diagonal compression.

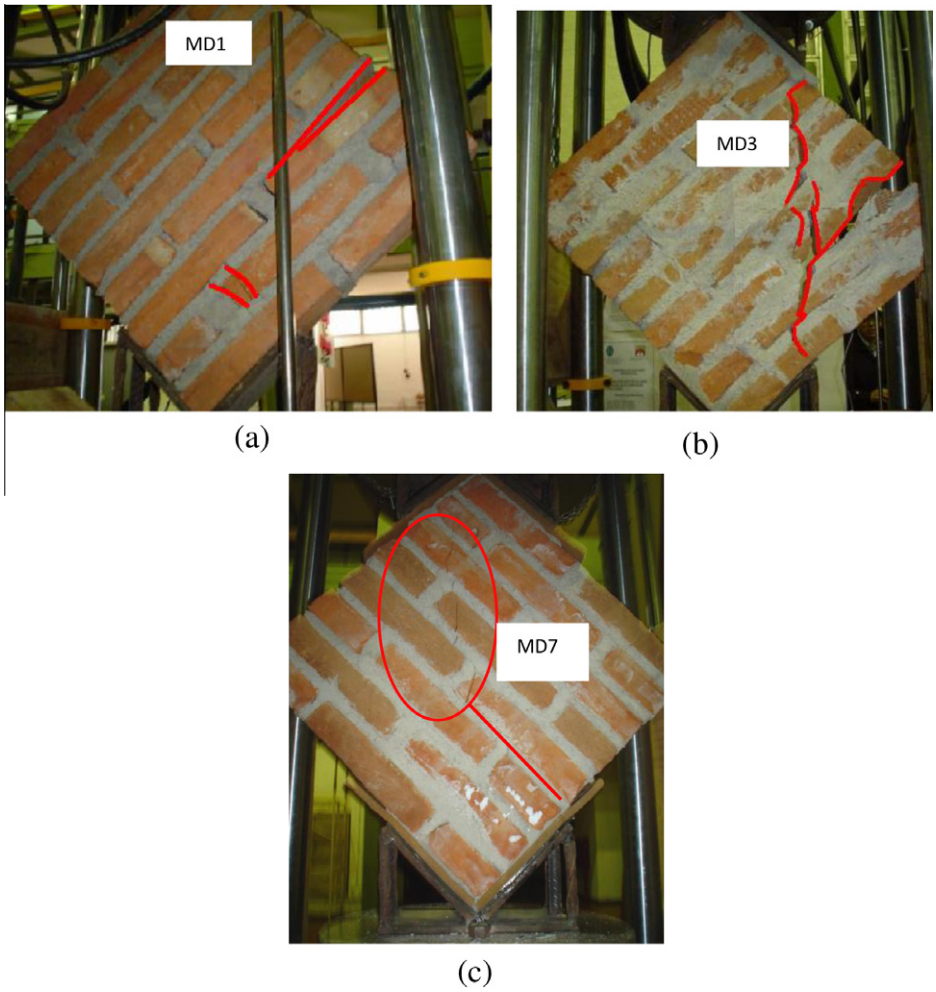

Fig. 13. Diagonal compression test. (a) MD1 failure mode. (b) MD3 failure mode. (c) MD7 failure mode.

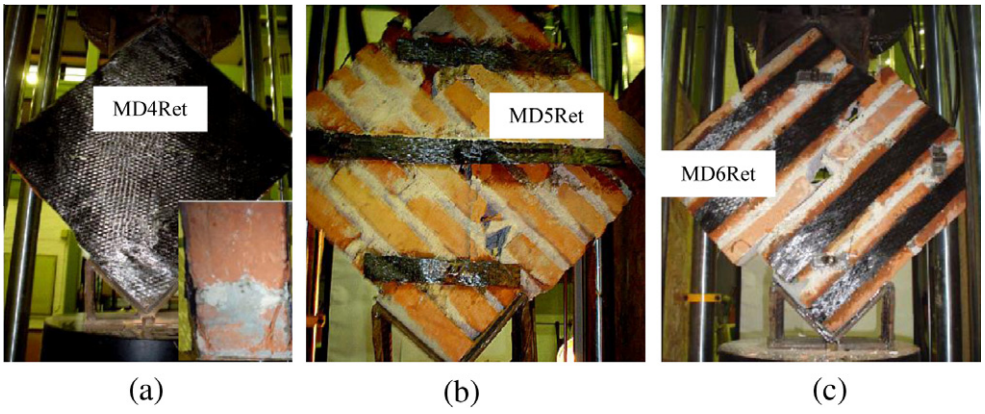

Fig. 14. Failure patterns of retrofitted panels under diagonal compression. (a) Completely retrofitted. (b) Retrofitted with diagonal bands. (c) Retrofitted with bands parallel to mortar joints.

improvement is hardly appreciable. All the specimens present a moderate increase of stiffness and increase of deformation capacity with strip length. Specimen MD9Ret fails abruptly for a load significantly lower than that expected. In this case, failure is produced by the sliding of central mortar joint resulting from the pull out of the central CFRP band evidencing a poor adhesion with masonry.

In general, failure is localized in the support zone as result of brick and mortar failure and in the case of shorter strips, the failure of superficial layers of the bricks that produces the pull out of the CFRP laminas is also observed. All panels preserve the monolithism after failure and they present a less brittle failure than the unreinforced specimens, depending on the anchorage length of the central band.

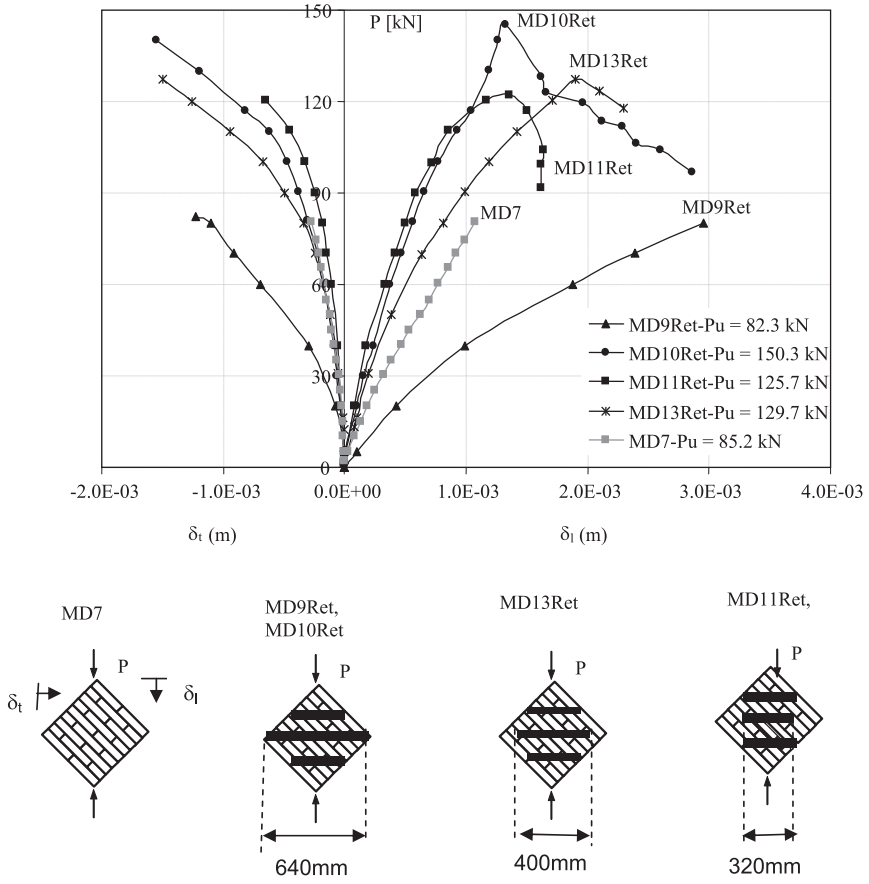

Fig. 15. Load–displacement curves for panels retrofitted with CFRP diagonal bands with variable length under diagonal compression.

Improvements in ultimate load of retrofitted specimens in comparison with reference specimens is presented in Fig. 16a, where reinforcement ratio is also shown. In Fig. 16b laminate area to panel face area ratio for specimens retrofitted with different band length is represented. One CFRP lamina of 1 mm final thickness applied to each surface of the panel is considered. It should be noted that, in spite of retrofitting band length and all the variability in materials properties observed, the improvement of strength is bounded between 50% and 100%.

4.2.3. Panels repaired with CFRP laminas

The load–displacement curves obtained for the repaired panels and the comparison with those corresponding to the unreinforced specimens are presented in Fig. 17. The post-peak response of MD8Rep and MD7Rep show their important deformation capability. Actually, all repaired specimens increase their deformation capacity, but the post-peak response is only recorded for MD8Rep and MD7Rep that kept their monolithism almost up to failure. In all the other cases, the measurement equipment was removed before failure to prevent it from damage caused by the collapse of the masonry specimens.

Specimens totally damaged and then repaired with CFRP, not only recover initial strength, but also exhibited a strength increase of about 30%. Brittle failure is initiated near the lower support and produces brick failure followed by the pull out of the CFRP laminas. Specimens preloaded to 50% of the failure load and then repaired, present an increase of about 70% in ultimate strength. Failure is similar to that presented by the other repaired specimens. Improvements in ultimate load of repaired specimens MD3Rep and MD7Rep in comparison with reference specimens are also shown in Fig. 16a and b, respectively.

5. Numerical analysis

5.1. Introduction

In order to study the behaviour of the retrofitted and repaired specimens and to calibrate a numerical tool for the analysis of this type of problem, all the specimens tested were modelled using finite element method and numerical results were compared with experimental results previously presented [42]. This numerical tool is used in this section for the analysis of the effect of bond width and length on the retrofitting efficiency.

A 2D non-linear finite element program developed by the authors for research purposes was used. Numerical results were compared with experimental ones. Triangular plane stress elements with three nodes were used for most of the simulations but, in order to reproduce the debonding of the CFRP laminas, some simulations were carried out with three dimensional models using tetrahedral elements with four nodes [24]. Typical finite element meshes used for a retrofitted panel under compression normal to bed joint and diagonal compression are presented in Fig. 18a and b respectively.

5.2. Constitutive models

A fine meshing of bricks and mortar was defined. An orthotropic plastic model was used both for bricks and mortar [43,44], with different values for the material constants in correspondence with material mechanical properties (Table 5). In the case of retrofitted or repaired specimens modelled in-plane stress, the sets of brick and CFRP lamina or mortar and CFRP lamina, were modelled with classical "mixture theory" (Voigt model) [45,46]. In this simplified

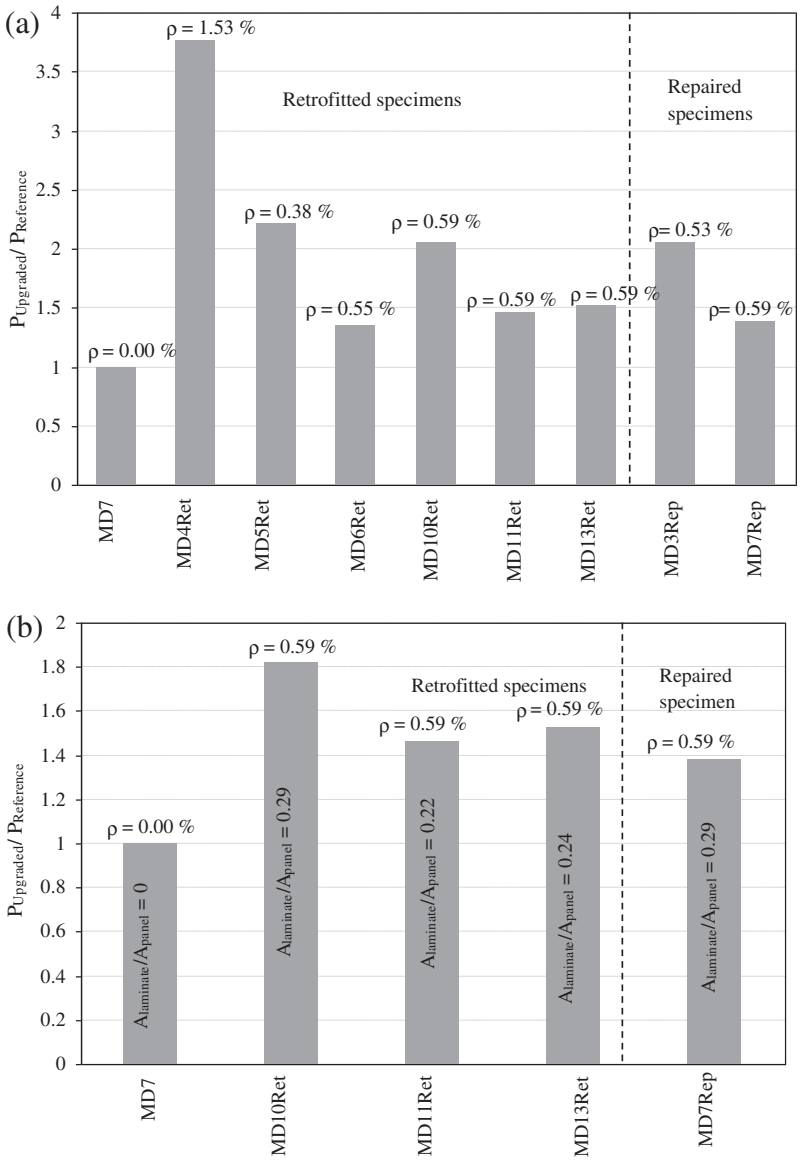

Fig. 16. Improvements in ultimate load of retrofitting specimens.

composite model all the components are assumed to have the same strains and the composite stress is obtained as the sum of the component stresses multiplied by their respective volume fractions. A general orthotropic elastoplastic model [47] was used for the CFRP lamina.

The orthotropic model used is based on the assumption that two spaces can be defined [48,49]: (a) a real anisotropic space and (b) a fictitious isotropic space. The problem is solved in the fictitious isotropic space allowing the use of elastoplastic models originally developed for isotropic materials. The isotropic elastoplastic model used in this paper includes energy-based criteria to make it suitable for brittle materials [43,44].

Stress tensors in both spaces are related by a tensor transformation that can be written as

$$\boldsymbol{\tau} = \boldsymbol{A}(\boldsymbol{\sigma}, \kappa^p) : \boldsymbol{\sigma} \tag{1}$$

where $\boldsymbol{\tau}$ and $\boldsymbol{\sigma}$ are the stress tensors in spaces (b) and (a) respectively, and $\boldsymbol{A}$ is a fourth order transformation tensor that contains the information about strength anisotropy depending on material symmetry. In the most general case, this tensor varies with the stress state and the evolution of the inelastic process represented by the isotropic plastic hardening variable κ^p [43]. In this paper, all the component materials were assumed initially isotropic or orthotropic with three axes of material symmetry. There are different alternatives to define tensor $\boldsymbol{A}$ for this case [49–53]. The simplest way is a diagonal fourth order tensor [46],

$$A_{ijkl} = \sum_{m=1}^{3}\sum_{n=1}^{3} \delta_{im}\delta_{jn}\delta_{km}\delta_{\ln}\bar{\tau}/\bar{\sigma}_{mn} \tag{2}$$

where $\bar{\tau}$ is the strength in the fictitious isotropic space and $\bar{\sigma}_{mn}$ is the actual strength in the direction $\boldsymbol{m}$ in the plane with normal $\boldsymbol{n}$. A better approach has been proposed by Oller et al. [53].

The plastic threshold is defined through a yielding function,

$$F(\boldsymbol{\sigma};\boldsymbol{\alpha}) = \bar{F}(\boldsymbol{\tau};\bar{\boldsymbol{\alpha}}) = 0 \tag{3}$$

where F and $\bar{F}$ represent the yielding function in the real anisotropic space and the fictitious isotropic space respectively; $\boldsymbol{\alpha}$ and $\bar{\boldsymbol{\alpha}}$ are plastic internal variables in correspondence with both spaces.

The transformation defined by Eq. (1) allows the use of yielding functions $\bar{F}$ defined for isotropic materials in the fictitious isotropic space. It should be noted that this space is isotropic with respect to

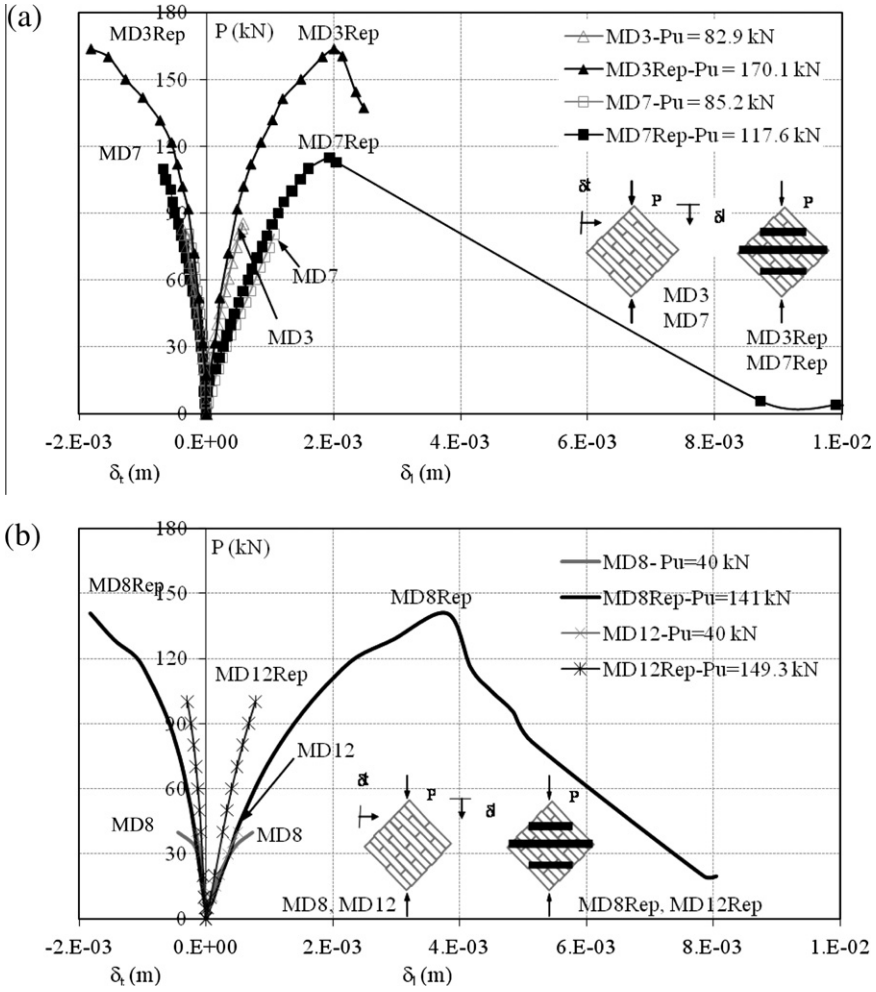

Fig. 17. Load–displacement curves for repaired specimens under diagonal compression. (a) MD3Rep and MD7Rep. (b) MD8Rep and MD12Rep.

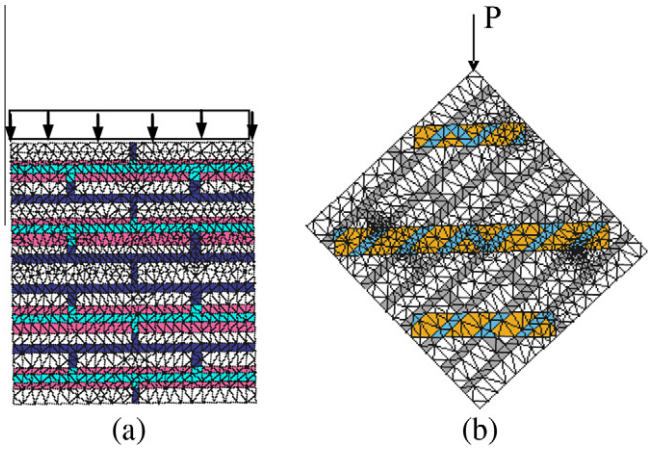

Fig. 18. CFRP retrofitted panels-finite element mesh. (a) Retrofitting with strips parallel to bed joints. (b) Retrofitting with strips orthogonal to load direction.

yielding thresholds and strength but not necessarily with respect to other properties like elastic stiffness.

The constitutive equation for an elastoplastic material can be written as follows:

$$\boldsymbol{\sigma} = \boldsymbol{C} : \boldsymbol{\varepsilon}^e = \boldsymbol{C} : (\boldsymbol{\varepsilon} - \boldsymbol{\varepsilon}^p) \tag{4}$$

where $\boldsymbol{C}$ is the elastic stiffness tensor, $\boldsymbol{\varepsilon}^e$ is the elastic strain tensor, $\boldsymbol{\varepsilon}$ is the strain tensor and $\boldsymbol{\varepsilon}^p$ is the plastic or inelastic strain tensor.

Evolution of plastic strain in real space is defined with the well-known flow rule,

$$\dot{\boldsymbol{\varepsilon}}^p = \dot{\lambda}(\partial G/\partial \boldsymbol{\sigma}) \tag{5}$$

where G is the plastic potential function defined in the real stress space. Instead of working with this function that should be anisotropic, function $\overline{G}$ defined in the fictitious isotropic space could be used.

$$G(\boldsymbol{\sigma}, \boldsymbol{\alpha}) = \overline{G}(\boldsymbol{\tau}, \bar{\boldsymbol{\alpha}}) \tag{6}$$

Eq. (5) can then be rewritten as,

$$\dot{\boldsymbol{\varepsilon}}^p = \dot{\lambda}(\partial \overline{G}/\partial \boldsymbol{\sigma}) = \dot{\lambda}(\partial \overline{G}/\partial \boldsymbol{\tau}) : (\partial \boldsymbol{\tau}/\partial \boldsymbol{\sigma}) = \dot{\lambda}(\partial \overline{G}/\partial \boldsymbol{\tau}) : \boldsymbol{A}$$
$$\boldsymbol{H} = \dot{\lambda}\bar{\boldsymbol{h}} \quad \text{with} \quad \boldsymbol{H} = \partial \boldsymbol{\tau}/\partial \boldsymbol{\sigma} \quad \text{and} \quad \bar{\boldsymbol{h}} = (\partial \overline{G}/\partial \boldsymbol{\tau}) : \boldsymbol{H} \tag{7}$$

where $\boldsymbol{H}$ is a fourth-rank tensor and $\bar{\boldsymbol{h}}$ is a second-rank tensor and represents the plastic flow in the real orthotropic space.

Mechanical properties used for the CFRP lamina are presented in Table 6.

5.3. Uniaxial compression normal to the bed joints

The panels retrofitted with bands parallel to bed joints and normal to the applied load were numerically analyzed. The study variable was the width of the reinforcement strips. Masonry panels reinforced with unidirectional bands of constant length, but variable width (50 mm, 70 mm and 560 mm) were analyzed. Load–axial and transverse total displacements diagrams and their

Table 5
Bricks and mortar mechanical properties.

Specimens properties	580 × 610 × 130 (mm^3)			560 × 550 × 125 (mm^3)	
	Mortar (a)	Mortar (b)	Brick	Mortar	Brick
Elasticity modulus, E (MPa)	3380	4312	1662	1528	1400
Poisson's ratio, v	0.21	0.21	0.16	0.21	0.15
Tension ultimate strength, σ_{ut} (MPa)	0.673	0.772	0.591	0.54	0.414
Compression ultimate strength, σ_{uc} (MPa)	6.73	7.72	10.60	4	8.28
Uniaxial compression elastic threshold, σ_{fc} (MPa)	5.60	6.4	–	3.5	–
Initial compression/tension strength ratio, R_0^p	10	10	20	10	20
Plastic damage variable for the peak stress, κ_{comp}^p	0.20	0.20	–	0.20	–
Fracture energy, G_f^p (MPa m)	6.01-5	4.01-5	3.0E−5	1.01-5	3.0E−5
Crushing energy, G_c^p (MPa m)	6.01-3	4.01-3	2.0E−3	1.01-3	2.0E−3
Yield criterion	Mohr Coulomb	Mohr Coulomb	Drucker–Parger	Mohr Coulomb	Drucker–Parger
Plastic flow	Mohr Coulomb	Mohr Coulomb	Drucker–Parger	Mohr Coulomb	Drucker–Parger
Damage criteria	Drucker–Prager	Drucker–Prager	Drucker–Prager	Drucker–Prager	Drucker–Prager
Friction angle for damage function (°)	7	7	7	7	7
Uniaxial compression damage threshold, σ_c^d (MPa)	5.9	7.0	10	3.7	7.5
Damage fracture energy, G_d (MPa m)	6.0E−3	6.0E−3	5.0E−2	6.0E−3	5.0E−2

Table 6
Composite mechanical properties.

Volume fraction of fibres, k_f	0.3
Longitudinal elasticity modulus, E_l (MPa)	72,500
Transversal elasticity modulus, E_t (MPa)	6200
Longitudinal–transversal Poisson's ratio, v_{lt}	0.08
Transversal–longitudinal Poisson's ratio, v_{tl}	0.017
Transversal–transversal Poisson's ratio, v_{tt}	0.20
Longitudinal tensile strength, σ_{long}^u (MPa)	960
Transverse tensile strength, σ_t^u (MPa)	51
Yield criterion	Tresca

comparison with experimental results of an unreinforced panel are shown in Fig. 19. It can be observed that, whatever the strip width is, even in the case of the panel entirely reinforced, the strength is not increased. On the other hand, the vertical deformation capacity is notably increased when the strip width increases. The latter can be clearly seen in Fig. 20a and b where maximum axial load (P_{max}) and maximum axial displacement (δ_l) versus strip width are respectively represented.

5.4. Diagonal compression

The behaviour of solid clay masonry panels, reinforced with unidirectional PRFC strips with different anchorage lengths is numerically analyzed in this section in order to define the best length to achieve the minimum cost-benefit relationship. Three strip lengths are analyzed: 420 mm (minimum length), 640 mm and 840 mm (total length of the tension diagonal). In all cases, the length of the other two strips is kept constant.

The load versus longitudinal and transverse displacements curves are presented in Fig. 21 together with the experimental results for the longest strip. It can be concluded that, the longer the central strip, the higher the maximum load reached. However, between the 420 mm and 640 mm strips there are no significant differences in strength values. Maximum load (P_{max}) achieved by the specimen versus anchorage length of strips reinforcement is presented in Fig. 22. There is no much difference in stiffness between the different retrofitting schemes. From Figs. 21 and 22 it can be concluded that the bond length L = 420 mm is appropriate and a minimum bond length based on bricks and mortar dimensions is proposed as follows,

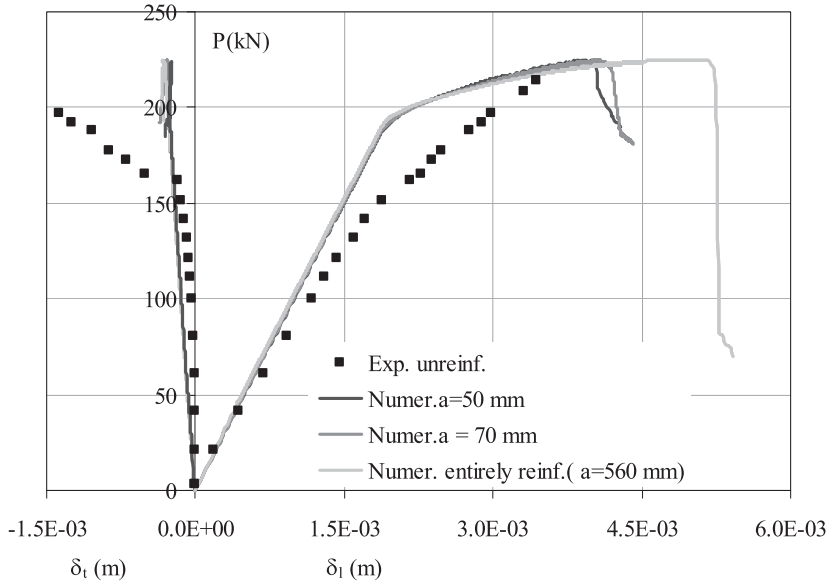

Fig. 19. Load versus axial and transverse displacement curves for panels with different CFRP retrofitting schemes under uniaxial compression.

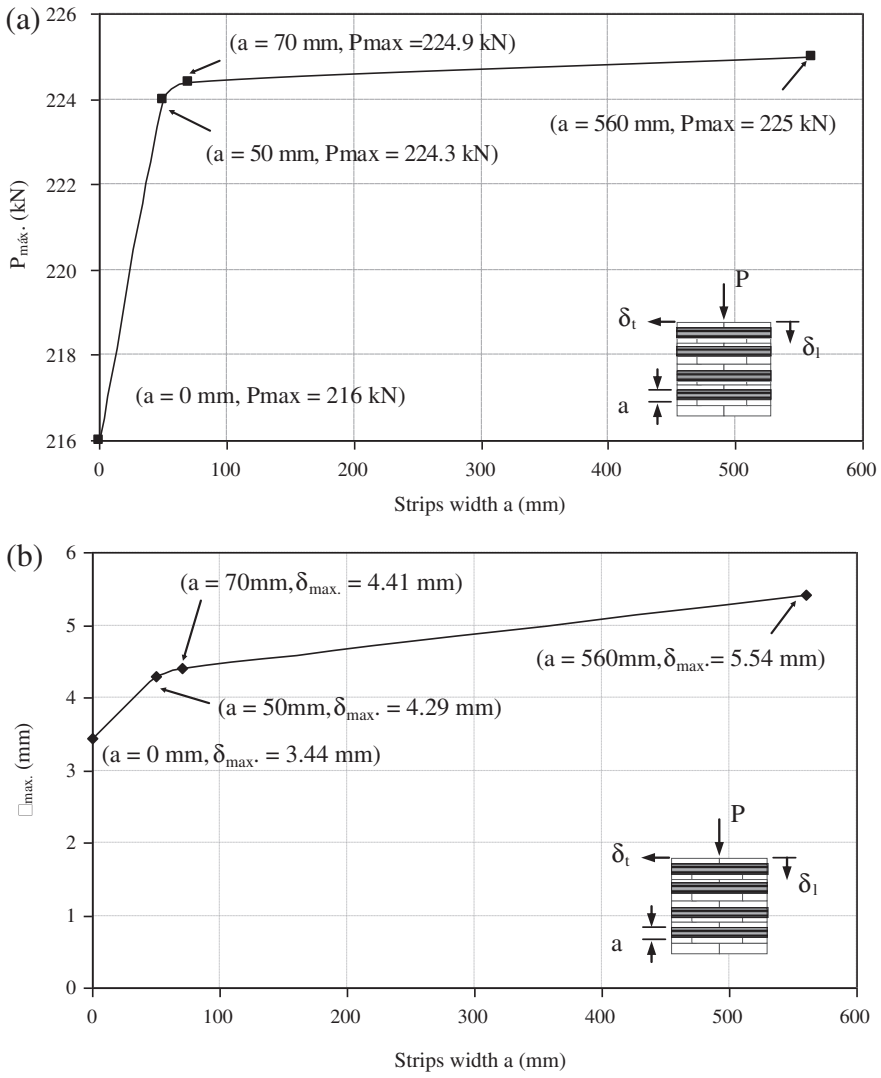

Fig. 20. Uniaxial compression test normal to the bed joints of CFRP strips reinforced masonry: (a) variation of the maximum axial load with the strips width; (b) variation of the maximum axial displacement with the strips width.

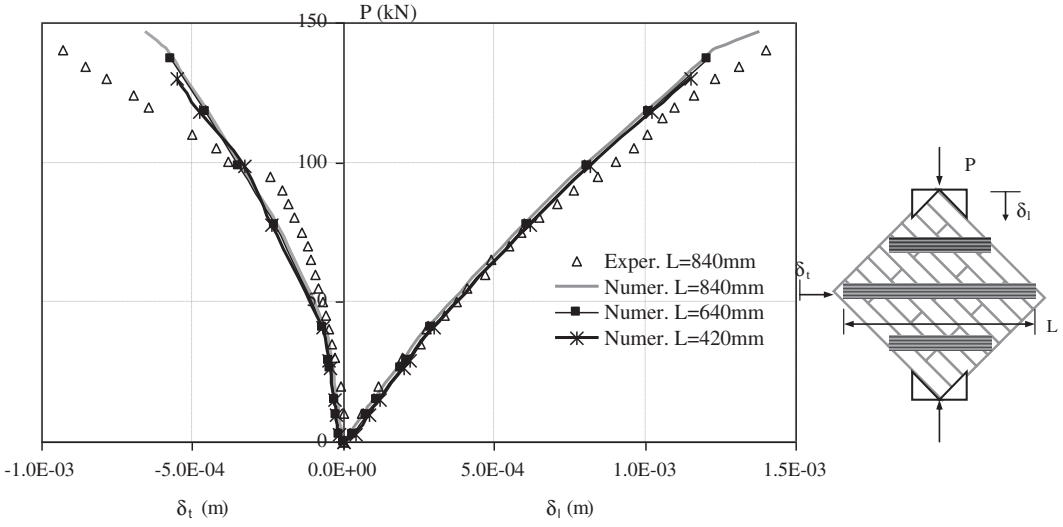

Fig. 21. Load versus axial and transverse displacements for CFRP strips retrofitted masonry panels under diagonal compression. Effect of central strip length.

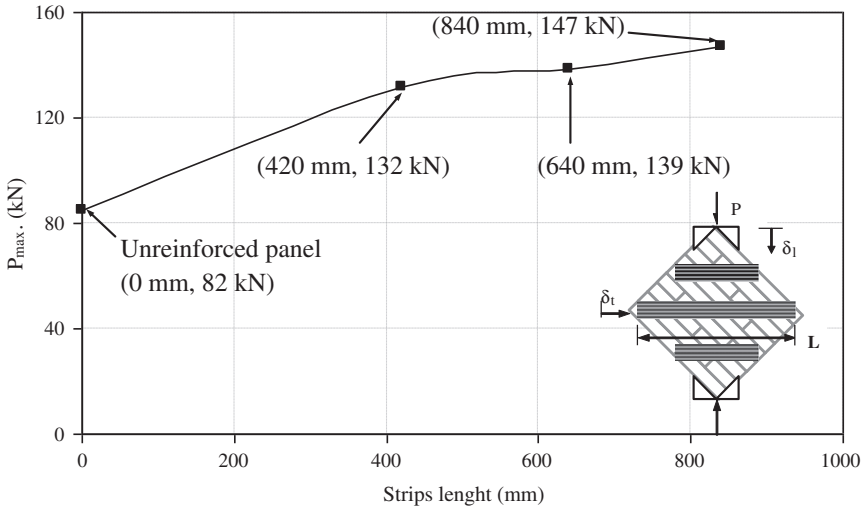

Fig. 22. Diagonal compression test corresponding to CFRP strips reinforcement masonry. Variation of maximum load with central strip lenght.

$$L_{min} = 2(\text{brick length} + \text{mortar thickness})\cos 45^{\circ} \quad (8)$$

6. Conclusions

The tests presented showed the efficiency of the retrofitting and repairing technique using CFRP.

From the analysis and comparison of experimental results, it can be concluded that if the correct retrofitting scheme is used, CFRP improves the behaviour of masonry, increasing ductility, ultimate strength and stiffness in some cases.

Although retrofitting with CFRP does not significantly increase strength under compression normal to bed joints, it improves ductility and failure mode. The increase in deformation capacity can reach 240% of the original value for total retrofitting. For this type of load, an optimum band width can be calculated. This width can be obtained from test results corresponding to specimens retrofitted with CFRP band of different widths and depends on the materials used and on the bricks and joints dimensions. The band should cover at least the joint width and part of the upper and lower bricks.

Depending on the dimensions and orientation, retrofitting with CFRP increases ductility under in-plane shear, prevents the joints sliding and increases the ultimate strength. In general, the increase in ultimate strength and deformation capacity found is higher than that reported by Gabor et al. [14] for specimens constructed with hollow clay bricks and retrofitted with bidirectional GFRP laminas and CFRP and GFRP bands. The increase in ultimate load is also higher than that obtained by Valluzzi et al. [9] for solid clay masonry panels retrofitted with CFRP bands.

Regarding the increase in load capacity and ductility, retrofitting with diagonal CFRP bands is effective and relatively economic when compared with total reinforcement. This fact is important when full sized walls must be retrofitted. Moreover, an optimum length of the reinforcing bands could be obtained in order to balance ductility and strength increase with the amount of CFRP. Some idea of the tendency of experimental results as a function of band length could be obtained from the series of specimens tested and numerical results presented. Based on experimental and numerical results a minimum bond length depending on brick and mortar dimensions is proposed. Nevertheless, more tests should be conducted to calculate the optimum band length.

Even though more tests are needed, it can be concluded that the specimens repaired behaved satisfactorily. This repairing technique presents the same benefits of the CFRP retrofitting. Most of the specimens repaired with CFRP bands presented an important improvement in ultimate load capacity and a considerable stiffness increase.

Actual building conditions (materials and workmanship) were intended to be reproduced in the tests. Conclusions obtained from these experimental results are valid for actual materials and construction techniques. Results presented in the paper should be interpreted taking into account this variability. Quantitative results are indicative of the improvement provided by the FRP retrofitting. Numerical values may vary as a consequence of this variability. Nevertheless, general conclusions stated in the paper are not expected to be affected by the observed variability.

Moreover, taking into account the brick and the reinforcement dimensions some size effect is likely to be expected when these small specimens are tested. Thus, much care should be taken in the direct extrapolation of the results to actual dimensions walls.

Acknowledgements

The authors wish to thank Sika (Argentina and Colombia) that provided the materials for the CFRP laminas and Ms. Amelia Campos for the English revision. The financial support of the National Scientific and Technological Research Council (CONICET), National University of Tucumán research Council (CIUNT) and National Technological University (UTN) is also acknowledged.

References

[1] Saadatmanesh H. Extending service life of concrete and masonry structures with fibre composites. Constr Build Mater 1997;11:327–35.
[2] ElGawady M, Lestuzzi P, Badoux M. In-plane seismic response of URM walls upgraded with FRP. J Compos Constr 2005;9(6):524–35.
[3] Ehsani M, Saadatmanesh H. Seismic retrofit of URM walls with fiber composites. TMS J 1996;14:63–72.
[4] Ehsani M, Saadatmanesh H, Al-Saidy A. Shear behavior of URM retrofitted with FRP overlays. J Compos Constr 1997;1(1):17–25.
[5] Ehsani M, Saadatmanesh H, Velazquez-Dimas J. Behavior of retrofitted URM walls under simulated earthquake loading. J Compos Constr 1999;3:134–42.
[6] Marshall O, Sweeney J, Trovillion J. Seismic rehabilitation of unreinforced masonry walls. ACI Special Publ 1999;188:287–96.
[7] Velazquez-Dimas J, Eshani M. Modeling out-of plane behavior of URM walls retrofitted with fiber composites. J Compos Constr 2000;4:172–81.
[8] Albert M, Elwi A, Cheng J. Strengthening of unreinforced masonry walls using FRPs. J Compos Constr 2001;5:76–84.
[9] Valluzzi M R, Tinazzi D, Modena C. Shear behavior of masonry panels strengthened by FRP laminates. Constr Build Mater 2002;16:409–16.
[10] Tumialan J, Galati N, Nanni A. Field assessment of unreinforced masonry walls strengthened with fiber reinforced polymer laminates. J Struct Eng 2003;129:1047–56.

[11] Chuang S, Zhuge Y, Wong T, Peters L. Seismic retrofitting of unreinforced masonry walls by FRP strips. In: Pacific conference on earthquake engineering; 2003.
[12] Tan K, Patoary M. Strengthening of masonry walls against out-of-plane loads using fiber-reinforced polymer reinforcement. J Compos Constr 2004;8:79–87.
[13] Gabor A, Ferrier E, Jacquelin E, Hamelin P. Analysis and modelling of the in-plane shear behavior of hollow brick masonry panels. Constr Build Mater 2006;20:308–21.
[14] Gabor A, Benani A, Jacquelin E, Lebon F. Modelling approaches of the in-plane shear behaviour of unreinforced and FRP strengthened masonry panels. Compos Struct 2006;74:277–88.
[15] Santa María H, Alcaino P, Luders C. Experimental response of masonry walls externally reinforced with carbon fiber fabrics. In: Proceedings of the 8th US national conference on earthquake engineering, San Francisco, California, USA; 2006.
[16] Prakash S, Alagusundaramoorthy P. Load resistance of masonry wallettes and shear triplets retrofitted with GFRP composites. Cem Concrete Compos 2008;30:745–61.
[17] Galati N, Tumialan G, Nanni A. Strengthening with FRP bars of URM walls subject to out-of-plane loads. Constr Build Mater 2006;20:101–10.
[18] ElGawady MA, Lestuzzi P, Badoux M. Static cyclic response of masonry walls retrofitted with fiber-reinforced polymers. J Compos Constr 2007;11(1):50–61.
[19] Camli US, Binic B. Strength of carbon fiber reinforced polymers bonded to concrete and masonry. Constr Build Mater 2007;21:1431–46.
[20] Willis CR, Yang Q, Seracino R, Griffith MC. Bond behaviour of FRP-to-clay brick masonry joints. Eng Struct 2009;31:2580–7.
[21] Capozucca R. Experimental FRP/SRP-historic masonry delamination. Compos Struct 2010;92:891–903.
[22] Willis CR, Yang Q, Seracino R, Griffith MC. Damaged masonry walls in two-way bending retrofitted with vertical FRP. Constr Build Mater 2009;23:1591–604.
[23] Roca P, Araiza G. Shear response of brick masonry small assemblages strengthened with bonded FRP laminates for in-plane reinforcement. Constr Build Mater 2010;24:1372–84.
[24] Luccioni B, Rougier V. Shear behaviour of brick mortar interface in CFRP retrofitted or repaired masonry. Int J Mech Sci 2010;52:602–11.
[25] Willis CR, Seracino R, Griffith MC. Out-of-plane strength of brick masonry retrofitted with horizontal NSM CFRP. Eng Struct 2010;32:547–55.
[26] Hamilton III H, Dolan C. Flexural capacity of glass FRP strengthened concrete masonry walls. J Compos Constr 2001;5:170–8.
[27] Hamoush S, Mcginley M, Mlakar P, Scott D, Murray K. Out-of plane-strengthening of masonry walls with reinforced composites. J Compos Constr 2001;5:139–45.
[28] Hamoush S, Mcginley M, Mlakar P, Terro M. Out-of plane-behavior of surface-reinforced masonry walls. Constr Build Mater 2002;16:341–51.
[29] El-Dakhakhni W, Hamid A, Hakam Z, Elgaaly M. Hazard mitigation and strengthening of unreinforced masonry walls using composites. Compos Struct 2005;73:458–77.
[30] Hamed E, Rabinovitch O. Failure characteristics of FRP-strengthened masonry walls under out-of-plane loads. Eng Struct 2010;32:2134–45.
[31] Benedetti A, Steli E. Analytical models for shear–displacement curves of unreinforced and FRP reinforced masonry panels. Constr Build Mater 2008;22:175–85.
[32] Chen Y, Ashour AF, Garrity SW. Moment/thrust interaction diagrams for reinforced masonry sections. Constr Build Mater 2008;22:763–70.
[33] Grande E, Milani G, Sacco E. Modelling and analysis of FRP-strengthened masonry panels. Eng Struct 2008;30:1842–60.
[34] Milani G, Milani E, Tralli A. Approximate limit analysis of full scale FRP-reinforced masonry building through a 3D homogenized FE package. Compos Struct 2010;92:918–35.
[35] Fedele R, Milani G. A numerical insight into the response of masonry reinforced by FRP strips. The case of perfect adhesion. Compos Struct 2010;92:2345–57.
[36] Su Y, Wu Ch, Griffth MC. Modelling of the bond–slip behavior in FRP reinforced masonry. Constr Build Mater 2011;25(1):328–34.
[37] Shrive NG. The use of fibre reinforced polymers to improve seismic resistance of masonry. Constr Build Mater 2006;20:269–77.
[38] Papanicolaou C, Triantafillou T, Lekka M. Externally bonded grids as strengthening and seismic retrofitting materials of masonry panels. Constr Build Mater 2011;25(2):504–14.
[39] INPRES-CIRSOC 103. Argentinian design rules for earthquake resistant buildings; 1991.
[40] Instituto Argentino de Racionalización de Materiales. IRAM 1622. Determinación de la resistencia a la compresión y a la flexión del cemento Portland; 1962.
[41] Instituto Argentino de Racionalización de Materiales. IRAM 12586. Ladrillos y bloques cerámicos para la construcción de muros, Método de ensayo de resistencia a la compresión; 2004.
[42] Rougier V. Refuerzo de muros de mampostería con materiales compuestos. PhD thesis, Universidad Nacional de Tucumán, Tucumán, Argentina; 2007.
[43] Luccioni B, Oller S, Danesi R. Coupled plastic-damaged model. Comput Method Appl Mech 1996;129:81–9.
[44] Luccioni B, Rougier V. A plastic damage approach for confined concrete. Comput Struct 2005;83:2238–56.
[45] Luccioni B. Constitutive model for fiber reinforced composite laminates. J Appl Mech Trans ASME 2006;73(6):901–10.
[46] Toledo M, Nallim L, Luccioni B. A micro-macromechanical approach for composite laminates. Mech Mater 2008;40:885–906.
[47] Luccioni B, Martín P. Modelo elastoplástico para materiales ortótropos. Rev Int Mét Numér Dis Cálc Ing 1996;13(4):603–14.
[48] Betten J. Application of tensor functions to the formulation of yield criteria for anisotropic materials. Int J Plast 1988;4:29–46.
[49] Luccioni B, Oller S, Danesi R. Plastic damaged model for anisotropic materials. Appl Mech Am 1995;I:124–9.
[50] Oller S, Botello S, Miquel M, Oñate E. Anisotropic elasto-plastic model based on an isotropic formulation. Eng Comput 1995;12:245–62.
[51] Luccioni B, Martín PE. Modelo elastoplástico para materiales ortótropos. Rev Int Mét Num Dis Cálc Ing 1997;13(4):603–14.
[52] Car E, Oller S, Oñate E. A large strain plasticity model for anisotropic composite material application. Int J Plast 1999;17(11):1437–63.
[53] Oller S, Car E, Lubliner J. Definition of a general implicit orthotropic yield criterion. Comput Method Appl Mech 2003;192:895–912.